Using Seismic Source Parameters to Model Frequency-Dependent Surface-Wave Radiation Patterns

Boris Rösler*[1] and Suzan van der Lee[1]

Abstract

The excitation of surface waves depends on the frequency-dependent eigenfunctions of the Earth, which are determined numerically. As a consequence, radiation patterns of Rayleigh and Love waves cannot be calculated analytically and vary with source depth and with frequency. Owing to the importance of surface-wave amplitudes for inversions of source processes as well as studies of the elastic and anelastic structure of the Earth, assessing surface-wave radiation patterns for different source mechanisms is desirable. A data product developed in collaboration with the Incorporated Research Institutions for Seismology (IRIS) Consortium provides visualizations of the radiation patterns for Rayleigh and Love waves for all possible source mechanisms. Radiation patterns for known earthquakes are based on the moment tensors reported by the Global Centroid Moment Tensor project. These source mechanisms can be modified or moment tensor components can be chosen by the user to assess their effect on Rayleigh- and Love-wave radiation patterns.

Cite this article as Rösler, B., and S. van der Lee (2020). Using Seismic Source Parameters to Model Frequency-Dependent Surface-Wave Radiation Patterns, *Seismol. Res. Lett.* **91**, 992–1002, doi: 10.1785/0220190128.

Introduction

Owing to the shear failure mechanisms of earthquakes, amplitudes of seismic waves vary with azimuth from the epicenter and with wavenumber. Radiation patterns of body waves can be expressed in analytic form (Aki and Richards, 2002). The formulae for the radiation patterns of surface waves (Ben-Menahem and Singh, 1981) depend on the fundamental-mode eigenfunctions at the depth of the hypocenter and coefficients determined by the strike ϕ_f, dip δ and slip angle λ of a double-couple (DC) source mechanism. For Rayleigh waves, the excitation functions $S_R(\omega)$, $P_R(\omega)$, and $Q_R(\omega)$ (Ben-Menahem and Israel, 1970) are derived from the radial eigenfunctions for spheroidal modes, and for Love waves, $P_L(\omega)$ and $Q_L(\omega)$ are derived from the radial eigenfunctions of toroidal modes evaluated at the source depth. The excitation functions determine the symmetry of radiation patterns: radiation patterns that only depend on $P_{R/L}(\omega)$ have a fourfold symmetry, a dependence on $Q_{R/L}(\omega)$ causes a twofold symmetric radiation pattern and radiation patterns depending only on $S_R(\omega)$ are circularly symmetric. Together with the fault geometry factors for Rayleigh waves

$$
\begin{aligned}
s_R(\phi) &= \sin\lambda \sin\delta \cos\delta \\
p_R(\phi) &= \cos\lambda \sin\delta \sin 2(\phi-\phi_f) - \sin\lambda \sin\delta \cos\delta \cos 2(\phi-\phi_f) \\
q_R(\phi) &= \sin\lambda \cos 2\delta \sin(\phi-\phi_f) + \cos\lambda \cos\delta \cos(\phi-\phi_f) \qquad (1)
\end{aligned}
$$

and Love waves

$$
\begin{aligned}
p_L(\phi) &= \sin\lambda \sin\delta \cos\delta \sin 2(\phi-\phi_f) + \cos\lambda \sin\delta \cos 2(\phi-\phi_f) \\
q_L(\phi) &= -\cos\lambda \cos\delta \sin(\phi-\phi_f) + \sin\lambda \cos 2\delta \cos(\phi-\phi_f), \qquad (2)
\end{aligned}
$$

the complex radiation pattern functions are

$$
\begin{aligned}
V_R(\omega,\phi) &= s_R(\phi)S_R(\omega) + p_R(\phi)P_R(\omega) + iq_R(\phi)Q_R(\omega) \\
V_L(\omega,\phi) &= p_L(\phi)P_L(\omega) + iq_L(\phi)Q_L(\omega), \qquad (3)
\end{aligned}
$$

in which ϕ is the azimuth to stations where they are observed. The amplitude and phase radiation patterns for Rayleigh waves at each frequency are obtained from the real and imaginary parts of $V_R(\omega,\phi)$ as

$$
\begin{aligned}
A_R(\omega,\phi) &= \sqrt{(s_R(\phi)S_R(\omega))^2 + (p_R(\phi)P_R(\omega))^2 + (q_R(\phi)Q_R(\omega))^2} \\
\Phi_R(\omega,\phi) &= \arctan\frac{q_R(\phi)Q_R(\omega)}{s_R(\phi)S_R(\omega) + p_R(\phi)P_R(\omega)}. \qquad (4)
\end{aligned}
$$

Similarly, the amplitude and phase radiation patterns for Love waves are

1. Department of Earth and Planetary Sciences, Northwestern University, Evanston, Illinois, U.S.A.

*Corresponding author: boris@earth.northwestern.edu

$$A_{\mathrm{L}}(\omega,\phi) = \sqrt{(p_{\mathrm{L}}(\phi)P_{\mathrm{L}}(\omega))^2 + (q_{\mathrm{L}}(\phi)Q_{\mathrm{L}}(\omega))^2}$$
$$\Phi_{\mathrm{L}}(\omega,\phi) = \arctan\frac{q_{\mathrm{L}}(\phi)Q_{\mathrm{L}}(\omega)}{p_{\mathrm{L}}(\phi)P_{\mathrm{L}}(\omega)}. \quad (5)$$

The excitation functions $S_{\mathrm{R}}(\omega)$, $P_{\mathrm{R/L}}(\omega)$, and $Q_{\mathrm{R/L}}(\omega)$ depend on the frequency-dependent eigenfunctions of the Earth, and hence the shapes of surface-wave radiation patterns may change over the frequency range of Rayleigh and Love waves. As a result, surface-wave radiation patterns are more difficult to derive than radiation patterns of body waves. However, radiation patterns of surface waves have been published for certain source mechanisms and frequencies (Haskell, 1953, 1963, 1964; Ben-Menahem, 1961, 1964), and can be used to infer the source mechanism of earthquakes. Because all research on surface waves depends on their radiation patterns, their understanding is important for data analysis and may influence conclusions in studies of surface waves.

Purpose

Surface-wave radiation patterns determine the amplitudes and phases of Rayleigh and Love waves in the far field of an earthquake and are intrinsically used in the research of surface waves. Because surface waves are often recorded with better signal-to-noise ratios (SNRs) in seismograms than body waves, surface-wave spectra as a function of azimuth have been used in inversions for source processes assuming a DC mechanism to obtain the strike, dip, and slip angle on a fault plane (Ben-Menahem and Toksöz, 1962, 1963a, 1963b; Wu and Ben-Menahem, 1965; Abe, 1970, 1972a, 1972b; Kanamori, 1970a, 1970b; Ben-Menahem *et al.*, 1972; Wu and Kanamori, 1973; Kanamori and Cipar, 1974; Singh *et al.*, 1975; Yoshioka and Abe, 1976; Herrmann, 1978; Stein and Okal, 1978; Herrmann *et al.*, 1980; Lay *et al.*, 1982; Romanowicz and Suárez, 1983; Zhang and Lay, 1990a, 1992; Beckers and Lay, 1995) or to further constrain focal mechanisms obtained by other methods (Lay and Kanamori, 1980; Zhang and Lay, 1990b; Velasco *et al.*, 1993). Radiation patterns have also proven to be useful to derive other source parameters such as the source depth (Tsai and Aki, 1970), seismic moment (Furumoto and Fukao, 1976; Chen and Molnar, 1977; Niazi and Kanamori, 1981), rupture length (Zhang and Kanamori, 1988) and velocity, and stress drop. The constraints on different fault parameters are obtained by comparing the observed radiation pattern to theoretically derived surface-wave amplitudes for different sources and by comparing the spectra of synthetic seismograms and of observed waveforms. Radiation patterns can also be used to distinguish DC from other source types and point sources from sources with finite length. Deriving moment tensors for historic earthquakes relies strongly on an understanding of surface-wave amplitude radiation as they help explain the observed amplitudes in analog seismograms. Structural seismologists use surface-wave recordings as constraints on 3D varying Earth structure (e.g., waveform fitting, group- and phase-velocity dispersion measurements, and amplifying and attenuating properties of the crust and upper mantle) and require a good SNR and an understanding of expected signal amplitudes. Data selection is facilitated by knowledge of the location of nodes in the radiation patterns of the different types of surface waves. Radiation patterns can be used to distinguish between natural and anthropogenic sources such as explosions (Brune and Pomeroy, 1963; Liebermann and Pomeroy, 1969; Tsai and Aki, 1971; Aki and Tsai, 1972; Ekström *et al.*, 2012) and serve to monitor the nuclear-test-ban treaty by governmental agencies. High-amplitude surface waves have been related to dynamic triggering of small local seismic events, suggesting that radiation patterns might hold predictive power over where dynamic triggering might occur after a large earthquake (Miyazawa and Mori, 2005; Rubinstein *et al.*, 2007; Gomberg *et al.*, 2008; Miyazawa and Brodsky, 2008; Miyazawa *et al.*, 2008; Peng and Chao, 2008; Peng *et al.*, 2008, 2009, 2013; Ghosh *et al.*, 2009; Guilhem *et al.*, 2010; Fry *et al.*, 2011; Chao *et al.*, 2012, 2013; Gonzalez-Huizar *et al.*, 2012; Chao and Obara, 2016).

Because of the dependence on the eigenfunctions of the Earth, radiation patterns of surface waves vary with frequency. Therefore, they are more difficult to derive and require more effort to compute than those of body waves. Given their importance for source and structural seismology, easy access to surface-wave radiation patterns for different source mechanisms is desirable.

Methodology

Seismic sources

Typical earthquakes are modeled by slip on a fault between tectonic plates characterized by the strike and dip of the fault plane and the slip angle. These angles describe a DC focal mechanism, which can be expressed mathematically as a symmetric moment tensor with vanishing trace and two equal, nonzero, but opposite eigenvalues. Moment tensors can also be used to represent other types of seismic events with nonzero isotropic components (Ross *et al.*, 2015; Okal *et al.*, 2018) or with compensated linear vector dipole (CLVD) components (Julian, 1983; Sipkin, 1986; Ross *et al.*, 1996; Julian *et al.*, 1997, 1998; Miller *et al.*, 1998; Vavryčuk, 2002; Shuler *et al.*, 2013), especially on nonplanar faults (Frohlich, 1994). From the fault angles for pure DC sources, moment tensor components are calculated as (Aki and Richards, 2002)

$$\begin{aligned}
M_{rr} &= \sin\lambda\sin 2\delta\\
M_{\theta\theta} &= -\sin\delta\cos\lambda\sin 2\phi_f - \sin 2\delta\sin\lambda(\sin\phi_f)^2\\
M_{\varphi\varphi} &= \sin\delta\cos\lambda\sin 2\phi_f - \sin 2\delta\sin\lambda(\cos\phi_f)^2\\
M_{r\theta} &= -\cos\delta\cos\lambda\cos\phi_f - \cos 2\delta\sin\lambda\sin\phi_f\\
M_{r\varphi} &= \cos\delta\cos\lambda\sin\phi_f - \cos 2\delta\sin\lambda\cos\phi_f\\
M_{\theta\varphi} &= -\sin\delta\cos\lambda\cos 2\phi_f - \frac{1}{2}\sin 2\delta\sin\lambda\sin 2\phi_f. \quad (6)
\end{aligned}$$

Radiation patterns

Kanamori and Given (1981) found analytic expressions for fundamental-mode Rayleigh- and Love-wave radiation pattern functions of seismic sources in terms of their moment tensor components

$$
\begin{aligned}
V_{\mathrm{R}}(\omega,\phi) &= P_{\mathrm{R}}(\omega)[M_{\theta\varphi}\sin 2\phi + \frac{1}{2}(M_{\varphi\varphi} - M_{\theta\theta})\cos 2\phi] \\
&+ \frac{1}{3}[S_{\mathrm{R}}(\omega) + N_{\mathrm{R}}(\omega)]M_{rr} + \frac{1}{6}[2N_{\mathrm{R}}(\omega) - S_{\mathrm{R}}(\omega)](M_{\theta\theta} + M_{\varphi\varphi}) \\
&+ iQ_{\mathrm{R}}(\omega)(M_{r\theta}\cos\phi - M_{r\varphi}\sin\phi) \\
V_{\mathrm{L}}(\omega,\phi) &= P_{\mathrm{L}}(\omega)\left[\frac{1}{2}(M_{\theta\theta} - M_{\varphi\varphi})\sin 2\phi + M_{\theta\varphi}\cos 2\phi\right] \\
&- iQ_{\mathrm{L}}(\omega)(M_{r\theta}\sin\phi + M_{r\varphi}\cos\phi). \qquad (7)
\end{aligned}
$$

Because moment tensors can describe isotropic seismic sources, the radiation pattern functions for non-DC sources depend not only on the numerically derived excitation functions $S_{\mathrm{R}}(\omega)$, $P_{\mathrm{R/L}}(\omega)$, and $Q_{\mathrm{R/L}}(\omega)$, but also on a function that describes the excitation of isotropic sources $N_{\mathrm{R}}(\omega)$. Because isotropic sources do not excite Love waves, only the Rayleigh-wave radiation pattern function includes this function.

The complex radiation pattern functions can be written as a linear combination of the moment tensor components and the Fourier transform of Green's functions computed for each of the moment tensor components. After grouping terms by moment tensor component following Dahlen (1980) and Dziewonski and Woodhouse (1983), the complex radiation patterns are

$$
V_{\mathrm{R/L}}(\omega,\phi) = \sum_{i=1}^{6} M_i \tilde{G}_{\mathrm{R/L},i}(\omega), \qquad (8)
$$

in which M_i are the moment tensor components M_{rr}, $M_{\theta\theta}$, $M_{\varphi\varphi}$, $M_{r\theta}$, $M_{r\varphi}$, and $M_{\theta\varphi}$, and

$$
\begin{aligned}
\tilde{G}_{\mathrm{R},rr}(\omega,\phi) &= \frac{1}{3}S_{\mathrm{R}}(\omega) + \frac{1}{3}N_{\mathrm{R}}(\omega) & \tilde{G}_{\mathrm{L},rr}(\omega,\phi) &= 0 \\
\tilde{G}_{\mathrm{R},\theta\theta}(\omega,\phi) &= -\frac{1}{2}P_{\mathrm{R}}(\omega)\cos 2\phi - \frac{1}{6}S_{\mathrm{R}}(\omega) + \frac{1}{3}2N_{\mathrm{R}}(\omega) & \tilde{G}_{\mathrm{L},\theta\theta}(\omega,\phi) &= \frac{1}{2}P_{\mathrm{L}}(\omega)\sin 2\phi \\
\tilde{G}_{\mathrm{R},\varphi\varphi}(\omega,\phi) &= \frac{1}{2}P_{\mathrm{R}}(\omega)\cos 2\phi - \frac{1}{6}S_{\mathrm{R}}(\omega) + \frac{1}{3}N_{\mathrm{R}}(\omega) & \tilde{G}_{\mathrm{L},\varphi\varphi}(\omega,\phi) &= -\frac{1}{2}P_{\mathrm{L}}(\omega)\sin 2\phi \\
\tilde{G}_{\mathrm{R},r\theta}(\omega,\phi) &= iQ_{\mathrm{R}}(\omega)\cos\phi & \tilde{G}_{\mathrm{L},r\theta}(\omega,\phi) &= -iQ_{\mathrm{L}}(\omega)\sin\phi \\
\tilde{G}_{\mathrm{R},r\varphi}(\omega,\phi) &= iQ_{\mathrm{R}}(\omega)\sin\phi & \tilde{G}_{\mathrm{L},r\varphi}(\omega,\phi) &= iQ_{\mathrm{L}}(\omega)\cos\phi \\
\tilde{G}_{\mathrm{R},\theta\varphi}(\omega,\phi) &= P_{\mathrm{R}}(\omega)\sin 2\phi & \tilde{G}_{\mathrm{L},\theta\varphi}(\omega,\phi) &= P_{\mathrm{L}}(\omega)\cos 2\phi \qquad (9)
\end{aligned}
$$

are the Green's functions for Rayleigh and Love waves, respectively. Summing the Green's functions weighted by the moment tensor components provides the complex spectrum for synthetic radiation patterns. The amplitude of the radiation patterns displayed in the data product represents their absolute value at each azimuth

$$
\begin{aligned}
&A_{\mathrm{R/L}}(\omega,\phi) \\
&= \sqrt{\left[\sum_{i=1}^{6} M_i \Re e(\tilde{G}_i(\omega,\phi))\right]^2 + \left[\sum_{i=1}^{6} M_i \Im m(\tilde{G}_i(\omega,\phi))\right]^2}. \qquad (10)
\end{aligned}
$$

Data product

For a given Earth model, surface-wave radiation patterns depend on the moment tensor components of the focal mechanism, the source depth, and the frequency of seismic waves. Using the spectra of the Green's functions $\tilde{G}_i(\omega,\phi)$ for elementary moment tensors and weighting them with the selected moment tensor components M_i, radiation patterns for Rayleigh and Love waves can be calculated efficiently for any source mechanism at different frequencies and source depths.

The Global Centroid Moment Tensor (CMT) project (Dziewonski *et al.*, 1981; Ekström *et al.*, 2012) has provided moment tensor solutions for thousands of events since 1976. Our data product provides plots of the radiation patterns for all earthquakes with moment magnitude $M_{\mathrm{w}} \geq 6.0$ in the catalog of the Global CMT project for the provided CMT and centroid source depths, but negligible half-duration. The precomputed radiation patterns of the event-based data product are accompanied by the interactive data product that allows users to enter source parameters of their choice or modify the source parameters of known events to display the radiation patterns for Rayleigh and Love waves. Though being an independent product, the interactive product can be accessed from the event page of the static product to visualize changes in the radiation patterns caused by changes in the source parameters of the earthquake.

Their amplitudes in the data product are displayed as a function of azimuth for frequencies of the fundamental Rayleigh and Love waves in the surface-wave range (Fig. 1) calculated for a spherically symmetric nonrotating Earth (Gilbert, 1971). Like the Global CMT project, we assume a point source and do not take into account directivity effects.

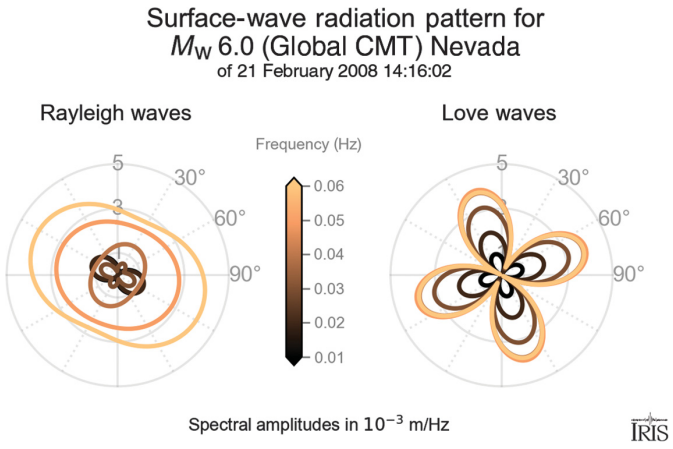

Figure 1. Radiation patterns of the Nevada earthquake on 21 February 2008.

Because surface-wave radiation patterns generated for different Earth models show only small differences in the absolute amplitudes and are practically indistinguishable from each other in the relative amplitudes, we provide a database for the model iasp91 (Snoke, 2009), a 1D seismic-velocity model that has been constructed to replicate the travel-time characteristics of seismic body waves.

The database of this data product contains the complex spectra of Green's functions of displacement at virtual stations located at an epicentral distance of 10° from the epicenter. At this distance, near-field effects are negligible and the radiation pattern reflects only far-field effects (Aki and Richards, 2002). Attenuation along the seismic-wave propagation and geometric spreading have been taken into account during their calculation.

Magnitude

For each provided source mechanism, the moment magnitude is calculated from the DC component of the moment tensor (Aki and Richards, 2002). Together with the isotropic and CLVD component, the DC component composes the moment tensor of an earthquake. After removing the isotropic component of the moment tensor as

$$\mathbf{M}_{\mathrm{dev}} = \mathbf{M} - \mathbf{M}_{\mathrm{iso}}, \tag{11}$$

in which $\mathbf{M}_{\mathrm{iso}} = \frac{1}{3}(M_{rr} + M_{\theta\theta} + M\varphi\varphi)\mathbf{I}$, we decompose the deviatoric moment tensor into a DC and a CLVD moment tensor (Knopoff and Randall, 1970)

$$\mathbf{M}_{\mathrm{dev}} = \mathbf{M}_{\mathrm{DC}} + \mathbf{M}_{\mathrm{CLVD}}. \tag{12}$$

For the moment tensor decomposition, we determine the eigenvalues $M_1 > M_2 > M_3$ of the deviatoric moment tensor $\mathbf{M}_{\mathrm{dev}}$. The eigenvalues of the DC moment tensor $\mathbf{M}_{\mathrm{DC}}$ are then M_0 and $-M_0$, and the seismic moment is determined from the dominant eigenvalues as (Dziewonski and Woodhouse, 1983)

$$M_0^{\mathrm{DC}} = \frac{1}{2}(|M_1| + |M_3|). \tag{13}$$

The seismic moment of the CLVD component follows as

$$M_0^{\mathrm{CLVD}} = |M_2|. \tag{14}$$

With the scalar moment of the DC component M_0 in Nm, the moment magnitude of an earthquake is obtained as (Kanamori, 1977; Hanks, 1979)

$$M_{\mathrm{w}} = \frac{2}{3}(\log M_0^{\mathrm{DC}} - 9.1). \tag{15}$$

Discussion

Surface-wave radiation patterns have been calculated for theoretical source mechanisms since 1964 when Haskell (1963) showed the influence of the dip and slip angle on the amplitudes of Rayleigh waves. Our data product allows calculating the radiation patterns of both Rayleigh and Love waves for any source that can be represented as a moment tensor. While it is obvious that the orientation of the radiation pattern changes with the strike ϕ_f of the fault on which the earthquake occurs, the influence of the dip angle δ, the slip angle λ, the hypocentral depth, and the frequency of seismic waves is more complex. The lobe patterns change with hypocentral depth because each frequency component is excited with a different amplitude.

Influence of dip angle

The Tohoku earthquake on 11 March 2011 occurred on a shallowly dipping reverse fault with a strike of $\phi_f = 203°$ and a dip of $\delta = 10°$ at a depth of 20 km as reported by the Global CMT project. Its surface-wave radiation pattern is typical for a reverse fault with the nodes of the Rayleigh-wave radiation pattern aligned perpendicular to the fault and the antinodes of the Love-wave radiation pattern aligned along the direction of the fault (Fig. 2). Although the shapes of the radiation patterns do not change with the frequency of the seismic waves for this source mechanism, the amplitudes increase with frequency.

To assess the influence of the dip angle of the fault plane on the radiation patterns of surface waves, we decompose the moment tensor of the earthquake into a DC and a CLVD component. Because the Global CMT project assumes a vanishing isotropic component for all source mechanisms, the reported moment tensors are purely deviatoric. The eigenvectors of the DC moment tensor are its seismic moment M_0 and its opposite $-M_0$. If $\mathbf{Q}$ is a square matrix constructed from the eigenvectors of $\mathbf{M}_{\mathrm{DC}}$, the DC component of the moment tensor is

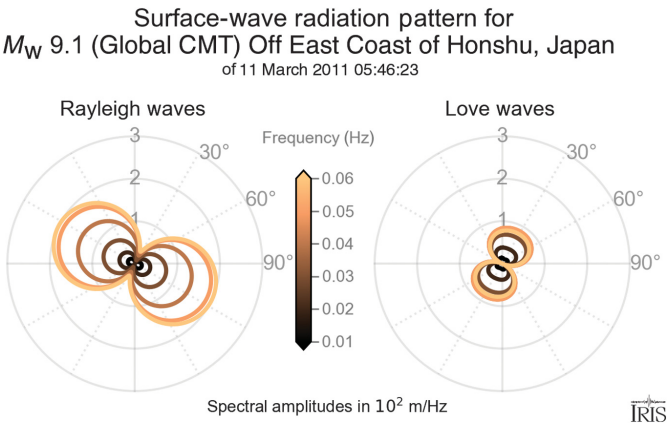

Figure 2. Radiation patterns of the Tohoku earthquake on 11 March 2011.

$$\mathbf{M}_{\mathrm{DC}} = \mathbf{Q}\boldsymbol{\Lambda}\mathbf{Q}^{-1}, \tag{16}$$

in which $\boldsymbol{\Lambda}$ is a diagonal matrix with the eigenvalues of the DC moment tensor M_1, M_2, and M_3 on its diagonal. The CLVD component of the moment tensor is then given as

$$\mathbf{M}_{\mathrm{CLVD}} = \mathbf{M}_{\mathrm{dev}} - \mathbf{M}_{\mathrm{DC}}. \tag{17}$$

By calculating DC moment tensors for different dip angles from equation (6) and adding the CLVD component of the moment tensor to it, we can modify the orientation of the fault plane of the DC component without changing the CLVD component. The radiation patterns for source mechanisms with a varying dip angle reveal that the steepness of the fault on which an earthquake occurs has influence on the shapes of the radiation patterns for both Rayleigh and Love waves. Nodal planes disappear for Rayleigh waves and appear for Love waves as the dip angle increases up to 45° after which the shapes of the radiation patterns change in the opposite way, setting constraints on the orientation of the fault plane (Fig. 3).

Influence of slip angle

The M_w 6.2 earthquake that occurred in Yemen on 13 December 1982 was one of the largest ever recorded in the country and due to its small source depth of 10 km, it caused severe destruction and numerous casualties. Its focal mechanism was a typical normal fault ($\lambda = 86°$) on a northwest-striking fault ($\phi_f = 320°$) with a dip angle of $\delta = 53°$ (Fig. 4).

The influence of a varying slip angle can be addressed when decomposing the moment tensor and changing the orientation of the slip vector of the DC component while leaving the orientation of the fault plane unchanged. By changing the slip angle, the source changes from a normal fault to a left-lateral strike-slip fault, and the shape of the radiation

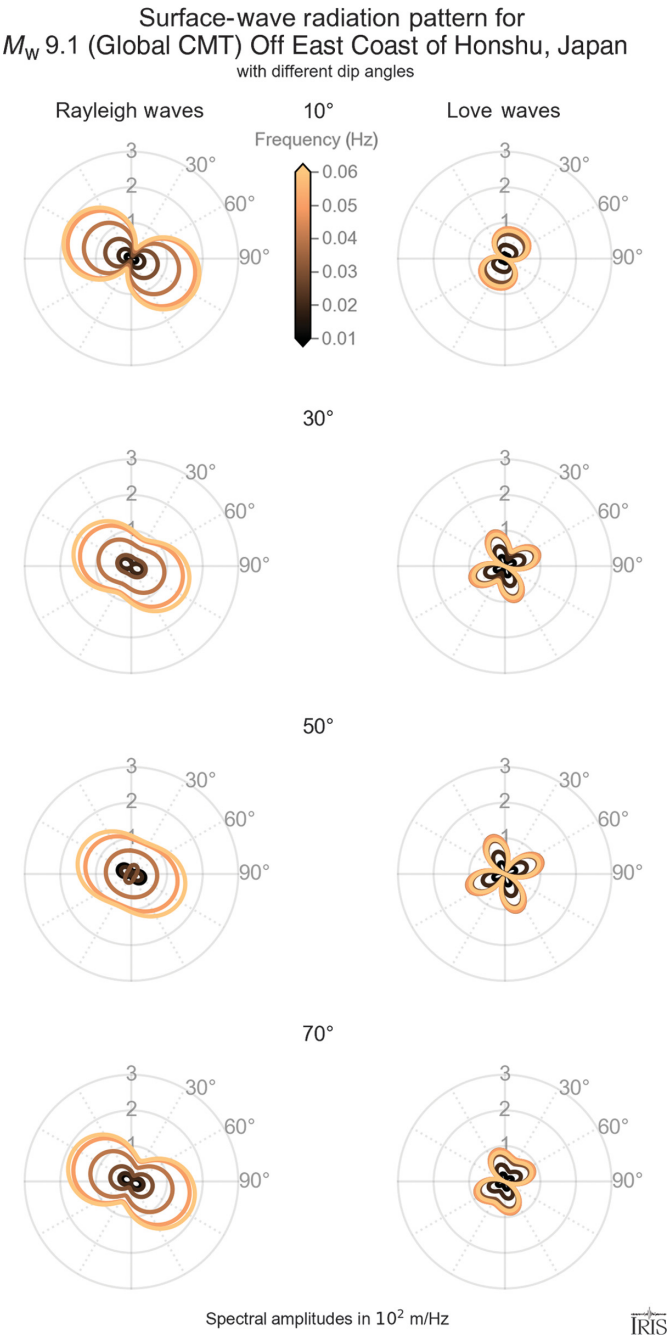

Figure 3. Influence of the dip angle on the radiation patterns of the Tohoku earthquake on 11 March 2011.

pattern of Rayleigh waves change significantly while the radiation pattern of Love waves merely varies in orientation and amplitude (Fig. 5).

The radiation patterns of earthquakes on reverse and normal faults have the same radiation pattern, and earthquakes on right- and left-lateral strike-slip faults generate the same surface-wave amplitudes when not considering their phase. This reflects the invariance of surface-wave radiation patterns to inversions of the slip vector, mathematically expressed as a

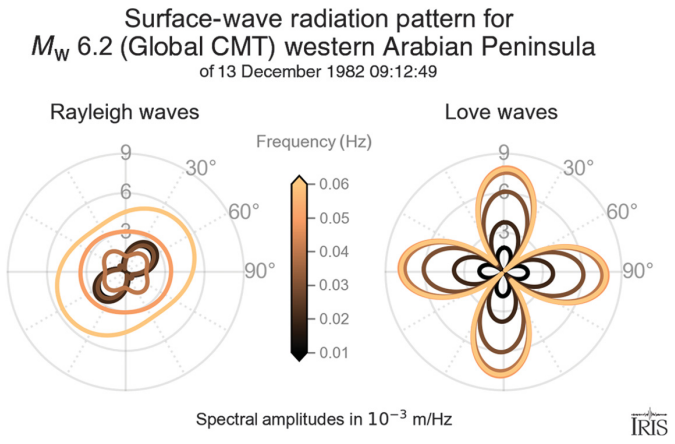

Figure 4. Radiation patterns of the Yemen earthquake on 13 December 1982.

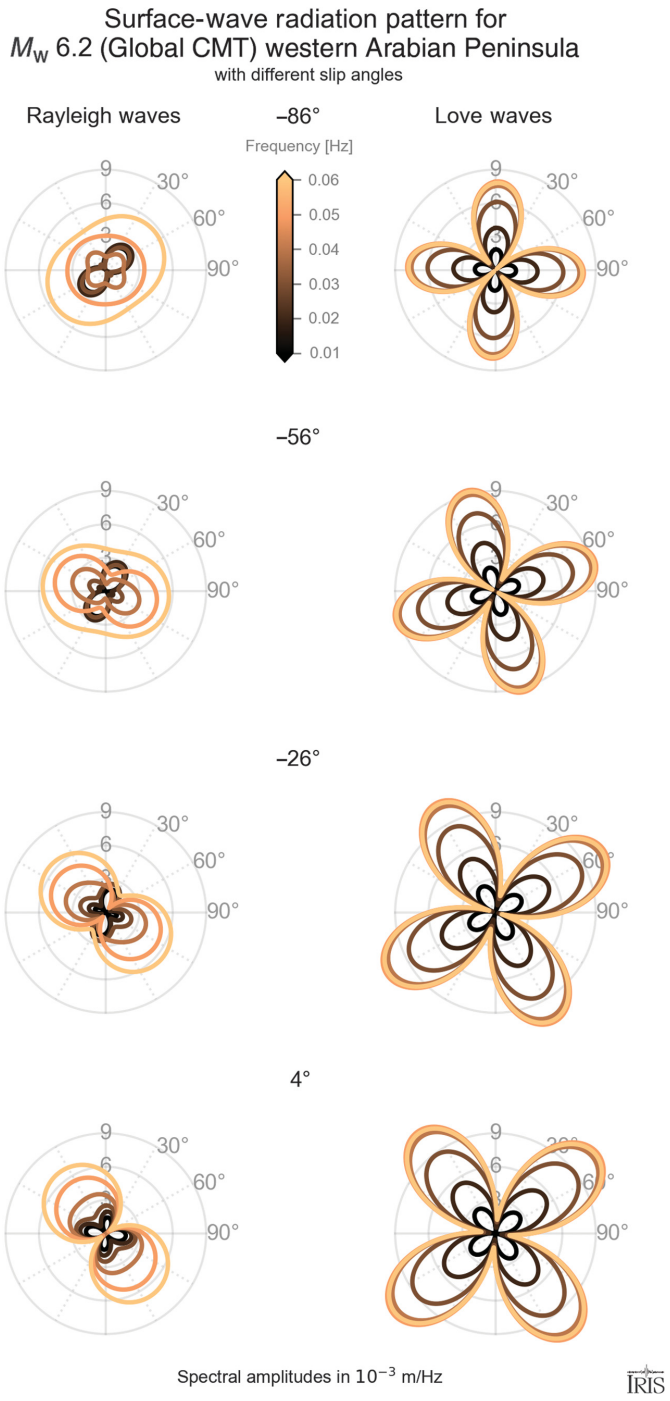

Figure 5. Influence of the slip angle on the radiation patterns of the Yemen earthquake on 13 December 1982.

change in the slip angle λ by 180°. This statement is true for arbitrary dip angles δ and strike angles ϕ_f.

Influence of source depth

The 24 May 2013 earthquake in the Sea of Okhotsk was the largest deep earthquake ever recorded and had a source depth of 611 km. Because of its deep source, the amplitudes of Rayleigh and Love waves are the largest for low frequencies (Fig. 6). Compared to the amplitudes at 0.01 Hz, the radiation patterns nearly vanish for other frequencies.

The source depth has a significant influence on the radiation patterns: the amplitudes of both Rayleigh and Love waves increase for smaller source depths and are dominated by high frequencies (Fig. 7). This change can be observed for all earthquakes at different source depths.

Observed source mechanisms

Iraq–Iran border region earthquake. The earthquake that occurred in the border region between Iraq and Iran on 12 November 2017 was caused by motion on a reverse fault shallowly dipping ($\delta = 11°$) to the northeast ($\phi_f = 351°$). With a slip angle of $\lambda = 140°$, the motion on the fault consisted of oblique thrust with components of right-lateral strike-slip motion (Talebian and Jackson, 2004). Despite its complicated source mechanism, the surface-wave radiation patterns of this earthquake with two lobes perpendicular to the fault for Rayleigh waves and along the fault for Love waves (Fig. 8) are typical for a reverse fault. For the source mechanism of this earthquake, the shapes of the radiation patterns do not depend on the frequency of the seismic waves. As expected for shallow earthquake sources, its amplitudes are largest for high frequencies.

Northridge earthquake. The Northridge earthquake that occurred on 17 January 1994 caused significant damage despite its moderate moment magnitude of M_w 6.6. A previously undiscovered fault, now named the Northridge blind-thrust fault, generated the highest ground acceleration ever recorded in an urban area in North America (Trifunac *et al.*, 1994). The source mechanism of this earthquake had a strike of $\phi_f = 130°$, a dip of $\delta = 42°$, and a slip of $\lambda = 116°$ (Thio and Kanamori, 1996) and was hence a combination between a thrust fault and a right-lateral strike-slip fault. The shapes of the radiation

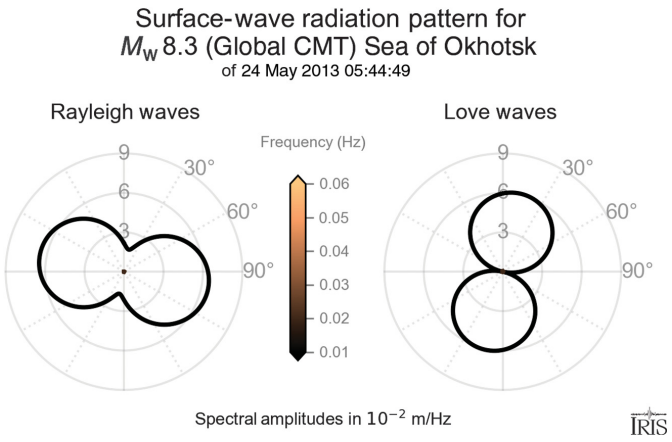

Figure 6. Radiation patterns of the Okhotsk earthquake on 24 May 2013.

patterns for Rayleigh and Love waves differ significantly for this earthquake: Love waves have a four-lobed radiation pattern whose shape does not change with frequency while Rayleigh waves change from a two-lobed to a single-lobed radiation pattern with increasing frequency. The shape of the Rayleigh-wave radiation pattern changes as the orientation of its nodal planes changes while the nodal planes of the radiation pattern of Love waves remains constant (Fig. 9).

Kaikōura earthquake. On 13 November 2016, an earthquake with a complex source mechanism ruptured at least six faults on the South Island of New Zealand. Its CMT was reported as a combination between oblique thrust and a right-lateral strike slip (Cesca *et al.*, 2017; Lo *et al.*, 2018). Both the radiation patterns of Rayleigh and Love waves change slightly with frequency for this earthquake. Although the orientation of the nodal planes of the two-lobed radiation pattern of Rayleigh waves changes, they have the same orientation for all frequencies in the Love-wave radiation pattern. However, Love waves have no clear nodes for higher frequencies, distinguishing this earthquake from most other source mechanisms (Fig. 10). Frequency-dependent nodal-plane orientations are usually observed for source mechanisms with significant CLVD component. The complex source mechanism of the Kaikōura earthquake has been modeled as a CMT with a large CLVD component whose moment amounts to 17% of the seismic moment of the DC component. As a result, the shapes of the surface-wave radiation patterns of the Kaikōura earthquake vary most noticeably with frequency.

Conclusions

Surface-wave radiation patterns for DC source mechanisms can be obtained analytically from the strike and dip of the fault plane and the slip angle and the numerically derived excitation functions $S_R(\omega)$, $P_{R/L}(\omega)$, and $Q_{R/L}(\omega)$. Source mechanisms

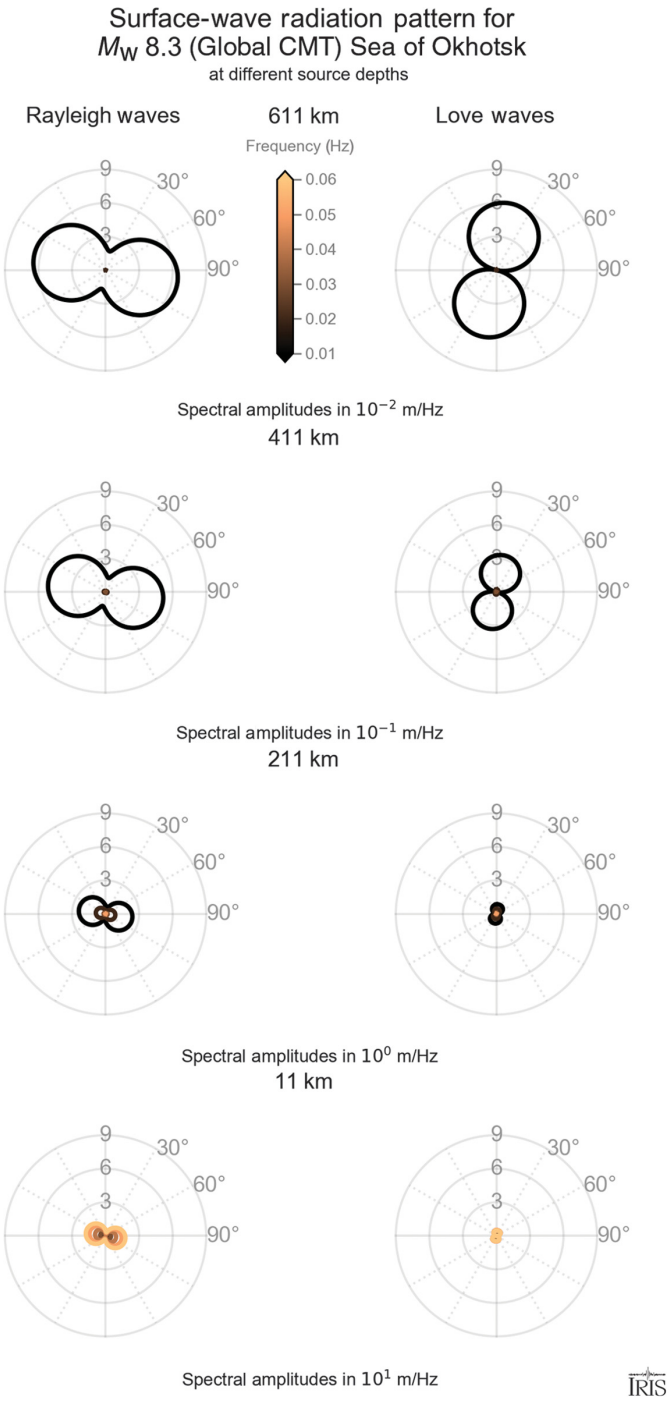

Figure 7. Influence of the source depth on the radiation patterns of the Okhotsk earthquake on 24 May 2013.

with an isotropic or a CLVD component have to be described as a moment tensor, and their Rayleigh- and Love-wave radiation patterns have to be computed from Green's functions. Based on the moment tensor components and the source depth, our surface-wave radiation pattern product displays the spectral amplitudes for both types of surface waves for different frequencies.

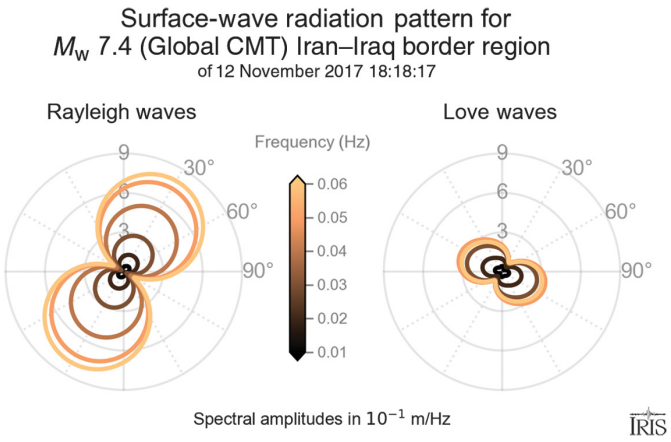

Figure 8. Radiation patterns of the Iraq–Iran border earthquake on 12 November 2017.

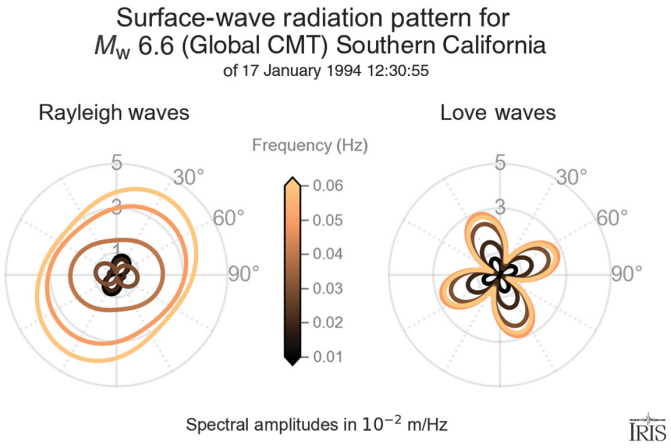

Figure 9. Radiation patterns of the Northridge earthquake on 17 January 1994.

The availability of the surface-wave radiation pattern product on Incorporated Research Institutions for Seismology's website can facilitate research on surface waves conducted by source and structural seismologists. Because the radiation patterns of Love and Rayleigh waves depend on the source process of the earthquake, amplitudes and phases of surface waves can help constrain the source mechanism. Both the source process and the Earth structure along the path of seismic-wave propagation have influence on the waveforms observed at seismic stations. Hence, the radiation pattern product can help separate the influence of the source process from path effects on seismic waves.

The shapes of the surface-wave radiation patterns may vary with the frequency of the seismic waves both for earthquakes with pure DC source mechanisms and other source types. The orientation of nodal planes does not vary with frequency for

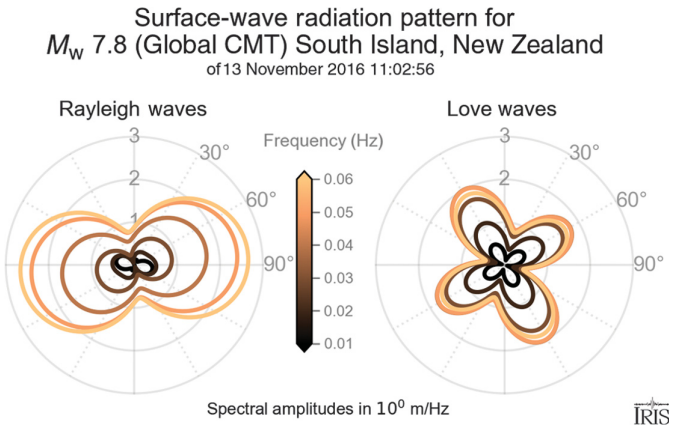

Figure 10. Radiation patterns of the Kaikōura earthquake on 13 November 2016.

DC source mechanisms, but is observed for earthquakes with a significant CLVD component. The hypocentral depth of an earthquake determines the frequency at which the amplitudes of surface waves are the largest. Shallow earthquakes have larger amplitudes for higher frequencies than deep earthquakes. However, earthquakes with a complex source mechanism have small surface-wave amplitudes at frequencies where the shapes of the radiation patterns change.

Data and Resources

We use spectral amplitudes for theoretical Green's functions to calculate the Rayleigh- and Love-wave amplitudes displayed in the Surface-Wave Radiation Pattern product. Its database has been generated with a modification of Mineos (Woodhouse, 1988), which computes surface-wave mode branches rather than normal modes for a spherically symmetric nonrotating Earth. Mineos is an open-source software whose source code is available through the website of the Computational Infrastructure for Geodynamics (https://geodynamics.org/cig/software/mineos/). All plots in this article are based on the Surface-Wave Radiation Pattern product, located at http://ds.iris.edu/ds/products/surface-wave-radiation-patterns/. All websites were last accessed on November 2019.

Acknowledgments

The development of this data product was inspired by Emily Wolin's idea to visualize surface-wave radiation patterns. The authors thank Frank Elavsky for his essential contribution to the programming of this data product and are grateful to Manochehr Bahavar, Adam Clark, Mick van Fossen, and Chad Trabant for their technical support and thoughtful comments about improving this product. The authors also thank Emile Okal for fruitful discussions about source mechanisms and the excitation of surface waves during the development of this data product. The Integrated Data-Driven Discovery in Earth and Astrophysical Sciences (IDEAS) Program of Northwestern University funded by National Science Foundation (NSF) Grant NRT 1450006 financially supported the development of this new data product.

References

Abe, K. (1970). Determination of seismic moment and energy from the earth's free oscillation, *Phys. Earth Planet. In.* **4,** no. 1, 49–61.

Abe, K. (1972a). Focal process of the South Sandwich Islands earthquake of May 26, 1964, *Phys. Earth Planet. In.* **5,** 110–122.

Abe, K. (1972b). Mechanics and tectonic implications of the 1966 and 1970 Peru earthquakes, *Phys. Earth Planet. In.* **5,** 367–379.

Aki, K., and P. G. Richards (2002). *Quantitative Seismology*, University Science Books, Sausalito, California.

Aki, K., and Y. B. Tsai (1972). Mechanism of Love-wave excitation by explosive sources, *J. Geophys. Res.* **77,** no. 8, 1452–1475.

Beckers, J., and T. Lay (1995). Very broadband seismic analysis of the 1992 Flores, Indonesia, earthquake ($M_w = 7.9$), *J. Geophys. Res.* **100,** no. B9, 18,179–18,193.

Ben-Menahem, A. (1961). Radiation of seismic surface-waves from finite moving sources, *Bull. Seismol. Soc. Am.* **51,** 401–435.

Ben-Menahem, A. (1964). Radiation patterns of seismic surface waves from buried dipolar point sources in a flat stratified Earth, *J. Geophys. Res.* **69,** no. 12, 2605–2620.

Ben-Menahem, A., and M. Israel (1970). Effects of major seismic events on the rotation of the Earth, *Geophys. J. Int.* **19,** no. 4, 367–393.

Ben-Menahem, A., and S. J. Singh (1981). *Seismic Waves and Sources*, Springer Verlag, New York, New York.

Ben-Menahem, A., and M. N. Toksöz (1962). Source-mechanism from spectra of long-period seismic surface-waves: 1. The Mongolian earthquake of December 4, 1957, *J. Geophys. Res.* **67,** no. 5, 1943–1955.

Ben-Menahem, A., and M. N. Toksöz (1963a). Source mechanism from spectrums of long-period surface waves: 2. The Kamchatka earthquake of November 4, 1952, *J. Geophys. Res.* **68,** no. 18, 5207–5222.

Ben-Menahem, A., and M. N. Toksöz (1963b). Source-mechanism from spectra of long-period seismic surface waves. 3. The Alaska earthquake of July 10, 1958, *Bull. Seismol. Soc. Am.* **53,** no. 5, 905–919.

Ben-Menahem, A., M. Rosenman, and M. Israel (1972). Source mechanism of the Alaskan earthquake of 1964 from amplitudes of free oscillations and surface waves, *Phys. Earth Planet. In.* **5,** 1–29.

Brune, J. N., and P. W. Pomeroy (1963). Surface wave radiation patterns for underground nuclear explosions and small-magnitude earthquakes, *J. Geophys. Res.* **68,** no. 17, 5005–5028.

Cesca, S., Y. Zhang, V. Mouslopoulou, R. Wang, J. Saul, M. Savage, S. Heimann, S.-K. Kufner, O. Oncken, and T. Dahm (2017). Complex rupture process of the Mw 7.8, 2016, Kaikoura earthquake, New Zealand, and its aftershock sequence, *Earth Planet. Sci. Lett.* **478,** 110–120, doi: 10.1016/j.epsl.2017.08.024.

Chao, K., and K. Obara (2016). Triggered tectonic tremor in various types of fault systems of Japan following the 2012 M_w 8.6 Sumatra earthquake, *J. Geophys. Res.* **121,** no. 1, 170–187.

Chao, K., Z. Peng, H. Gonzalez-Huizar, C. Aiken, B. Enescu, H. Kao, A. A. Velasco, K. Obara, and T. Matsuzawa (2013). A global search for triggered tremor following the 2011 M_w 9.0 Tohoku earthquake, *Bull. Seismol. Soc. Am.* **103,** no. 2B, 1551–1571.

Chao, K., Z. Peng, C. Wu, C. C. Tang, and C. H. Lin (2012). Remote triggering of non-volcanic tremor around Taiwan, *Geophys. J. Int.* 188, no. 1, 301–324.

Chen, W. P., and P. Molnar (1977). Seismic moments of major earthquakes and the average rate of slip in central Asia, *J. Geophys. Res.* **82,** no. 20, 2945–2969.

Dahlen, F. A. (1980). A uniformly valid asymptotic representation of normal mode multiplet spectra on a laterally heterogeneous Earth, *Geophys. J. Int.* **62,** no. 2, 225–247.

Dziewonski, A., and J. Woodhouse (1983). An experiment in systematic study of global seismicity: Centroid-moment tensor solutions for 201 moderate and large earthquakes of 1981, *J. Geophys. Res.* **88,** no. B4, 3247–3271.

Dziewonski, A. M., T. A. Chou, and J. H. Woodhouse (1981). Determination of earthquake source parameters from waveform data for studies of global and regional seismicity, *J. Geophys. Res.* **86,** 2825–2852.

Ekström, G., M. Nettles, and A. Dziewonski (2012). The global CMT project 2004-2010: Centroid-moment tensors for 13,017 earthquakes, *Phys. Earth Planet. In.* **200/201,** 1–9.

Frohlich, C. (1994). Earthquakes with non-double-couple mechanisms, *Science* **264,** no. 5160, 804–809.

Fry, B., K. Chao, S. Bannister, Z. Peng, and L. Wallace (2011). Deep tremor in New Zealand triggered by the 2010 M_w 8.8 Chile earthquake, *Geophys. Res. Lett.* **38,** no. 15, doi: 10.1029/2011GL048319.

Furumoto, M., and Y. Fukao (1976). Seismic moment of great deep shocks, *Phys. Earth Planet. In.* **11,** no. 4, 352–357.

Ghosh, A., J. E. Vidale, Z. Peng, K. C. Creager, and H. Houston (2009). Complex nonvolcanic tremor near Parkfield, California, triggered by the great 2004 Sumatra earthquake, *J. Geophys. Res.* **114,** no. B12, doi: 10.1029/2008JB006062.

Gilbert, F. (1971). Excitation of the normal modes of the Earth by earthquake sources, *Geophys. J. Roy. Astron. Soc.* **22,** no. 2, 223–226.

Gomberg, J., J. L. Rubinstein, Z. Peng, K. C. Creager, J. E. Vidale, and P. Bodin (2008). Widespread triggering of nonvolcanic tremor in California, *Science* **319,** no. 5860, 173.

Gonzalez-Huizar, H., A. A. Velasco, Z. Peng, and R. R. Castro (2012). Remote triggered seismicity caused by the 2011, M9.0 Tohoku-Oki, Japan earthquake, *Geophys. Res. Lett.* **39,** no. 10, 10,302.

Guilhem, A., Z. Peng, and R. Nadeau (2010). High-frequency identification of non-volcanic tremor triggered by regional earthquakes, *Geophys. Res. Lett.* **37,** no. 16, doi: 10.1029/2010GL044660.

Hanks, T. (1979). A moment magnitude scale, *J. Geophys. Res.* **84,** no. B5, 2348–2350.

Haskell, N. (1953). The dispersion of surface waves on multilayered media, *Bull. Seismol. Soc. Am.* **43,** 17–34.

Haskell, N. (1963). Radiation pattern of Rayleigh waves from a fault of arbitrary dip and direction of motion in a homogeneous medium, *Bull. Seismol. Soc. Am.* **53,** no. 3, 619–642.

Haskell, N. (1964). Radiation pattern of surface waves from point sources in a multi-layered medium, *Bull. Seismol. Soc. Am.* **54,** no. 1, 377–393.

Herrmann, R. B. (1978). A seismological study of two Attica, New York earthquakes, *Bull. Seismol. Soc. Am.* **68,** no. 3, 641–651.

Herrmann, R. B., J. W. Dewey, and S. K. Park (1980). The Dulce, New Mexico, earthquake of 23 January 1966, *Bull. Seismol. Soc. Am.* **70,** no. 6, 2171–2183.

Julian, B. R. (1983). Evidence for dyke intrusion earthquake mechanisms near Long Valley caldera, California, *Nature* **303,** no. 5915, 323.

Julian, B. R., A. D. Miller, and G. R. Foulger (1997). Non-double-couple earthquake mechanisms at the Hengill-Grensdalur volcanic complex, southwest Iceland, *Geophys. Res. Lett.* **24,** no. 7, 743–746.

Julian, B. R., A. D. Miller, and G. R. Foulger (1998). Non-double-couple earthquakes 1. Theory, *Rev. Geophys.* **36,** no. 4, 525–549.

Kanamori, H. (1970a). Synthesis ofzce studies—Kurile Islands earthquake of October 13, 1963, *J. Geophys. Res.* **75,** no. 26, 5011–5027.

Kanamori, H. (1970b). The Alaska earthquake of 1964: Radiation of long-period surface waves and source mechanism, *J. Geophys. Res.* **75,** no. 26, 5029–5040.

Kanamori, H. (1977). The energy release in great earthquake, *J. Geophys. Res.* **82,** no. 20, 2981–2987.

Kanamori, H., and J. J. Cipar (1974). Focal process of the great Chilean earthquake May 22, 1960, *Phys. Earth Planet. In.* **9,** no. 2, 128–136.

Kanamori, H., and J. W. Given (1981). Use of long-period surface waves for rapid determination of earthquake-source parameters, *Phys. Earth Planet. In.* **27,** no. 1, 8–31.

Knopoff, L., and M. J. Randall (1970). The compensated linear-vector dipole: A possible mechanism for deep earthquakes, *J. Geophys. Res.* **75,** no. 26, 4957–4963.

Lay, T., and H. Kanamori (1980). Earthquake doublets in the Solomon Islands, *Phys. Earth Planet. In.* **21,** no. 4, 283–304.

Lay, T., J. W. Given, and H. Kanamori (1982). Long-period mechanism of the 8 November 1980 Eureka, California, earthquake, *Bull. Seismol. Soc. Am.* **72,** no. 2, 439–456.

Liebermann, R. C., and P. W. Pomeroy (1969). Relative excitation of surface waves by earthquakes and underground explosions, *J. Geophys. Res.* **74,** no. 6, 1575–1590.

Lo, Y., L. Zhao, X. Xu, J. Chen, and S. Hung (2018). The 13 November 2016 Kaikoura, New Zealand earthquake: Rupture process and seismotectonic implications, *Earth Planet. Phys.* **2,** 139–149, doi: 10.26464/epp2018014.

Miller, A. D., G. R. Foulger, and B. R. Julian (1998). Non-double-couple earthquakes 2. Observations, *Rev. Geophys.* **36,** no. 4, 551–568.

Miyazawa, M., and E. E. Brodsky (2008). Deep low-frequency tremor that correlates with passing surface waves, *J. Geophys. Res.* **113,** no. B1, doi: 10.1029/2006JB004890.

Miyazawa, M., and J. Mori (2005). Detection of triggered deep low-frequency events from the 2003 Tokachi-oki earthquake, *Geophys. Res. Lett.* **32,** no. 10, doi: 10.1029/2005GL022539.

Miyazawa, M., E. E. Brodsky, and J. Mori (2008). Learning from dynamic triggering of low-frequency tremor in subduction zones, *Earth Planets Space* **60,** no. 10, e17–e20.

Niazi, M., and H. Kanamori (1981). Source parameters of 1978 Tabas and 1979 Qainat, Iran, earthquakes from long-period surface waves, *Bull. Seismol. Soc. Am.* **71,** no. 4, 1201–1213.

Okal, E., N. Saloor, S. H. Kirby, and M. Nettles (2018). An implosive component to the source of the deep Sea of Okhotsk earthquake of 24 May 2013: Evidence from radial modes and CMT inversion, *Phys. Earth Planet. In.* **281,** 68–78.

Peng, Z., and K. Chao (2008). Non-volcanic tremor beneath the Central Range in Taiwan triggered by the 2001 M_w 7.8 Kunlun earthquake, *Geophys. J. Int.* **175,** no. 2, 825–829.

Peng, Z., H. Gonzalez-Huizar, K. Chao, C. Aiken, B. Moreno, and G. Armstrong (2013). Tectonic tremor beneath Cuba triggered by the M_w 8.8 Maule and M_w 9.0 Tohoku-Oki earthquakes, *Bull. Seismol. Soc. Am.* **103,** no. 1, 595–600.

Peng, Z., J. E. Vidale, K. C. Creager, J. L. Rubinstein, J. Gomberg, and P. Bodin (2008). Strong tremor near Parkfield, CA, excited by the 2002 Denali fault earthquake, *Geophys. Res. Lett.* **35,** no. 23, doi: 10.1029/2008GL036080.

Peng, Z., J. E. Vidale, A. G. Wech, R. M. Nadeau, and K. C. Creager (2009). Remote triggering of tremor along the San Andreas fault in central California, *J. Geophys. Res.* **114,** no. B7, doi: 10.1029/2008JB006049.

Romanowicz, B., and G. Suárez (1983). On an improved method to obtain the moment tensor and depth of earthquakes from the amplitude spectrum of Rayleigh waves, *Bull. Seismol. Soc. Am.* **73,** no. 6A, 1513–1526.

Ross, A., G. R. Foulger, and B. R. Julian (1996). Non-double-couple earthquake mechanisms at the Geysers geothermal area, California, *Geophys. Res. Lett.* **23,** no. 8, 877–880.

Ross, Z. E., Y. Ben-Zion, and L. Zhu (2015). Isotropic source terms of San Jacinto fault zone earthquakes based on waveform inversions with a generalized CAP method, *Geophys. J. Int.* **200,** no. 2, 1269–1280.

Rubinstein, J. L., J. E. Vidale, J. Gomberg, P. Bodin, K. C. Creager, and S. D. Malone (2007). Non-volcanic tremor driven by large transient shear stresses, *Nature* **448,** no. 7153, 579.

Shuler, A., M. Nettles, and G. Ekström (2013). Global observation of vertical-CLVD earthquakes at active volcanoes, *J. Geophys. Res.* **118,** no. 1, 138–164.

Singh, D. D., B. K. Rastogi, and H. K. Gupta (1975). Surface-wave radiation pattern and source parameters of Koyna earthquake of December 10, 1967, *Bull. Seismol. Soc. Am.* **65,** no. 3, 711–731.

Sipkin, S. A. (1986). Interpretation of non-double-couple earthquake mechanisms derived from moment tensor inversion, *J. Geophys. Res.* **91,** no. B1, 531–547.

Snoke, J. A. (2009). Traveltime tables for iasp91 and ak135, *Seismol. Res. Lett.* **80,** no. 2, 260–262, doi: 10.1785/gssrl.80.2.260

Stein, S., and E. A. Okal (1978). Seismicity and tectonics of the Ninetyeast Ridge area: Evidence for internal deformation of the Indian plate, *J. Geophys. Res.* **83,** no. B5, 2233–2245.

Talebian, M., and J. Jackson (2004). A reappraisal of earthquake focal mechanisms and active shortening in the Zagros mountains of Iran, *Geophys. J. Roy. Astron. Soc.* **156,** no. 3, 506–526, doi: 10.1111/j.1365-246X.2004.02092.x.

Thio, H. K., and H. Kanamori (1996). Source complexity of the 1994 Northridge earthquake and its relation to aftershock mechanisms, *Bull. Seismol. Soc. Am.* **86,** no. 1B, S84–S92.

Trifunac, M. D., M. I. Todorovska, and S. S. Ivanović (1994). A note on distribution of uncorrected peak ground accelerations during the Northridge, California, earthquake of 17 January 1994, *Soil Dynam. Earthq. Eng.* **13,** no. 3, 187–196.

Tsai, Y. B., and K. Aki (1970). Precise focal depth determination from amplitude spectra of surface waves, *J. Geophys. Res.* **75,** no. 29, 5729–5744.

Tsai, Y. B., and K. Aki (1971). Amplitude spectra of surface waves from small earthquakes and underground nuclear explosions, *J. Geophys. Res.* **76,** no. 17, 3940–3952.

Vavryčuk, V. (2002). Non-double-couple earthquakes of 1997 January in West Bohemia, Czech Republic: Evidence of tensile faulting, *Geophys. J. Int.* **149,** no. 2, 364–373.

Velasco, A. A., T. Lay, and J. Zhang (1993). Long-period surface wave inversion for source parameters of the 18 October 1989 Loma Prieta earthquake, *Phys. Earth Planet. In.* **76,** nos. 1/2, 43–66.

Woodhouse, J. H. (1988). The calculation of the eigenfrequencies and eigenfunctions of the free oscillations of the Earth and the Sun, in *Seismological Algorithms*, D. J. Doornbos (Editor), Academic Press, London, United Kingdom, 321–370.

Wu, F. T., and A. Ben-Menahem (1965). Surface wave radiation pattern and source mechanism of the September 1, 1962, Iran earthquake, *J. Geophys. Res.* **70,** no. 16, 3943–3949.

Wu, F. T., and H. Kanamori (1973). Source mechanism of February 4, 1965, Rat island earthquake, *J. Geophys. Res.* **78,** no. 26, 6082–6092.

Yoshioka, N., and K. Abe (1976). Focal mechanism of the Iwate-Oki earthquake of June 12, 1968, *J. Phys. Earth*, **24,** no. 3, 251–262.

Zhang, J., and H. Kanamori (1988). Source finiteness of large earthquakes measured from long-period Rayleigh waves, *Phys. Earth Planet. In.* **52,** nos. 1/2, 56–84.

Zhang, J., and T. Lay (1990a). Source parameters of the 1989 Loma Prieta earthquake determined from long-period Rayleigh waves, *Geophys. Res. Lett.* **17,** no. 8, 1195–1198.

Zhang, J., and T. Lay (1990b). Effects of centroid location on determination of earthquake mechanisms using long-period surface waves, *Bull. Seismol. Soc. Am.* **80,** no. 5, 1205–1231.

Zhang, J., and T. Lay (1992). The April 5, 1990 Mariana Islands earthquake and subduction zone stresses, *Phys. Earth Planet. In.* **72,** nos. 1/2, 99–121.

Manuscript received 24 May 2019
Published online 2 January 2020